Spectral Tuning Mechanism of Photosynthetic Light-Harvesting Complex II Revealed by *Ab Initio* Dimer Exciton Model

Kazuhiro J. Fujimoto[†‡]*, *Takumi Minoda*[†], *and Takeshi Yanai*[†‡]*

[†] Institute of Transformative Bio-Molecules (WPI-ITbM), Nagoya University, Furocho, Chikusa, Nagoya 464-8601, Japan

[‡] Department of Chemistry, Graduate School of Science, Nagoya University, Furocho, Chikusa, Nagoya, 464-8601, Japan

Corresponding Authors

*Kazuhiro J. Fujimoto - Institute of Transformative Bio-Molecules (WPI-ITbM), Nagoya University, Furocho, Chikusa, Nagoya 464-8601, Japan; orcid.org/0000-0003-0286-3646; Email: fujimotok@chem.nagoya-u.ac.jp

*Takeshi Yanai - Institute of Transformative Bio-Molecules (WPI-ITbM), Nagoya University, Furocho, Chikusa, Nagoya 464-8601, Japan; orcid.org/0000-0003-3933-8546; Email: yanait@chem.nagoya-u.ac.jp

ABSTRACT

Excited states of two kinds of bacteriochlorophyll (BChl) aggregates, B850 and B800, in photosynthetic light-harvesting complex II (LH2) are theoretically investigated by developing and using an extended exciton model considering efficiently-evaluated excitonic coupling. Our exciton model based on dimer fragmentation is shown to reproduce the experimental absorption spectrum of LH2 with good accuracy, entailing their different redshifts originating from aggregations of B850 and B800. The systematic analysis has been performed on the spectra by quantitatively decomposing their spectral shift energies into the contributions of various effects: structural distortion, electrostatic, excitonic coupling, and charge-transfer (CT) effects. Our results show that the spectral redshift of B800 is mainly attributed to its electrostatic interaction with the protein environment, while that of B850 arises from the marked effect of the excitonic coupling between BChl units. The inter-chromophore CT excitation also plays a key role in the spectral redshift of B850. This CT effect can be effectively described using our dimer model. This suited characterization reveals that the pronounced CT effect originates from the characteristics of B850 that has closely-spaced BChls as dimers. We highlight an importance of the refinement of the crystal structure with use of quantum chemical methods for prediction of the spectrum.

(200 words)

1. INTRODUCTION

Molecular aggregates often exhibit optical absorption properties that are largely away from what we can simply deduce from the photophysical behaviors of the isolated monomeric molecule.[1-2] They may take different aggregation structures, which further diversify the spectral shape. An example of this is copper phthalocyanine (color index generic name: Pigment Blue 15),[3] which has two types of crystal structures, α-type and β-type. The absorption spectra of these two types significantly differ from each other as well as the spectrum of the gas-phase molecule.[4] The α-type crystal structure shows a reddish blue color, while the β-type structure shows a greenish blue color. Even if the crystals are composed of chemically identical molecules, the aggregates show different colors due to different forms of molecular packing in the crystals. Such remarkable aggregation effects on optical properties are similarly observed in biological molecular assemblies, [5-11] including light-harvesting complex II (LH2).[5-14]

LH2 is one of the antenna proteins found in purple photosynthetic bacteria.[12-14] The light energy collected by LH2 is transferred to light-harvesting I antenna and reaction center, and utilized for photosynthetic reactions.[15] LH2 contains many chromophores such as chlorophylls and carotenoids, and plays an important role as an efficient sunlight absorber.[16-18] Recently, an interesting attempt has been made to incorporate artificial chromophores into LH2 in order to further raise its light absorption efficiency.[19] The structure of LH2 antenna complex from *Rhodopseudomonas acidophila* consists of 27 bacteriochlorophyll *a* (BChl) that are arranged in two separate rings with different diameters (see **Figure 1ab**).[14] Such a characteristic aggregation is considered to lead to two large absorption peaks of LH2 redshifted from that of the monomer. The inner ring consisting of 18 BChls and the outer ring of 9 BChls are named B850 and B800, respectively, after the figures of their absorption peak wavelengths, 850 nm and 800 nm,

respectively.[15] B850 and B800 are in fact both composed of chemically identical compounds; thus, the formation of these different absorption peaks associated with B850 and B800 has posed a physicochemical question about its origin. A number of previous studies have gradually revealed the factors that contribute to the two peak shifts,[20-31] but the extent of their contributions is not well understood.

The changes in absorption wavelength due to the formation of molecular aggregates clearly reflects that the electronic structures of BChls are modulated by intermolecular interactions that take place across the complex. Dissecting the electronic-level mechanism of how the aggregations cause the spectral tuning requires us to perform excited state calculations on LH2 by handling the entire complex in an ideal manner. However, this task is generally difficult because the direct use of standard quantum chemical calculation is computationally formidable. The exciton model[32] is a powerful workaround. It is based on a scheme to use the product of separately-determined electronic states of molecular chromophore units. This effective separation of the assembly system allows for a significant reduction of computational costs and makes it applicable to large-scale systems.

A notable ingredient built into the exciton model is the effective inclusion of the interactions between the noninteracting subsystems to describe the entire interacting system. It is done through consideration of excitonic coupling (or electronic coupling), which is an intermediate physical quantity to account for intermolecular interaction mediated by quantum mechanical process between different electronic states of the subsystems. The excitonic coupling also serves as an important factor that determines the rate constant of excitation energy transfer (EET).[33] In the formalism of the exciton model, the excitonic coupling participates as the off-diagonal elements of the Hamiltonian matrix in the molecular unit bases. Obviously, the accuracy in the

determination of the excitonic couplings has a great influence on the prediction of the exciton model.

A widely-used approach to gauge excitonic coupling is the so-called dipole-dipole (DD) approximation using two transition dipoles because of its simplicity.[34] However, this method is properly applicable only when the intermolecular distance is larger than the molecular sizes.[35] Therefore, the DD method is ill-suited in case of studying molecular aggregates with small intermolecular distances like LH2 complex.

To circumvent the limitation of the DD method, various schemes for excitonic coupling calculation have been proposed.[36-49] One of the authors (K.J.F.) has proposed efficient schemes to compute excitonic coupling,[50-54] which were shown to enable a more accurate estimation and finer analysis of excitonic coupling compared to the DD method. In our previous studies, the exciton model based on the improved excitonic coupling methods was applied to photochemical and photobiological systems such as a retinal dimer,[51] xanthorhodopsin (XR),[50, 55] *Krokinobacter eikastus* rhodopsin 2 (KR2),[56] and tetracene crystal,[57] resulting in accurate reproduction of the characteristic absorption and CD spectra observed in the experiments.

There have been many attempts to reproduce the absorption spectrum of LH2 by computational approaches.[20-21, 23, 27-31] The research using the exciton model was pioneered by Hu et al.[20] and Alden et al.[21] In their calculations, the DD and semiempirical QCFF/PI methods were used to construct the exciton Hamiltonian but are seemingly inadequate for the aforementioned reason. Scholes et al.[23] applied the transition density cube (TDC) method[37] combined with the configuration interaction singles (CIS) transition densities to the excitonic coupling calculations and revealed that the excitonic coupling treatment beyond the DD level of theory is necessary for

guaranteeing the reliability of the exciton model applied to LH2. Recently, Li et al.[28], Cuppellini et al. [29], and Nottoli et al.[30] used the *ab initio* exciton model for LH2 and revealed an appreciable charge-transfer (CT) effect on the LH2 spectrum. As reviewed above, a number of the previous studies have been increasingly deepening the understanding of the factors that affect the simulated LH2 spectrum. Nonetheless, to the best of our knowledge, there is so far no study that has analyzed the spectral tuning mechanism of LH2 in terms of energy partitioning and quantitatively clarified the contribution of each energy component to the redshift.

In this study, we aim to scrutinize the spectral tuning mechanism of LH2 through extensive simulations including exciton calculations so as to distinctly account for BChl structural distortion effect, electrostatic effect, excitonic coupling effect, and CT effect. Detailed understanding of the aggregation effect on the spectrum is expected to be useful for artificial photosynthesis research.[6] Despite numerous theoretical studies on LH2 so far,[20-25, 28-31] the origin of the spectral tuning mechanism of LH2 remains unclear. The *ab initio* exciton study by Li et al.[28] showed a large redshift contribution to the absorption spectrum of B850 assembly by integrating the dimeric CT excited states in the monomeric exciton Hamiltonian; however, the predicted absorption wavelength for B850 was 775 nm, which differs from the experimental value (i.e., 850 nm) with an error of approximately 0.15 eV. Along a similar line, in this study, we introduce an alternative exciton treatment, designated the dimer exciton model, which can consider CT effects, for simulating the excited states of LH2 including B850 and B800. The dimer exciton model is based on the product of the electronic states of BChl dimers built on the dimer fragmentation. In this model, the excitation energy calculations of the non-interacting dimers are first performed to explicitly consider the inter-chromophore CT nature at the dimer level, followed by the inclusion of the excitonic coupling effects between the dimer units, which is done in the construction of the

exciton Hamiltonian of the interacting total system. It should be underscore that our dimer exciton model is a much simpler scheme than an approach by Li et al.[28] to include CT basis; this simplicity is rather beneficial for modeling complex aggregate systems containing a number of units such as LH2.

In addition to this exciton model, we shed light on the importance of the refinement of the crystal structure for the reliable *ab initio* prediction of the LH2 spectrum. To our best knowledge, there are no earlier first-principles studies that have investigated the effect of geometry optimization of the crystal structure on the excitation energies of LH2. We have carried out the structural refinement of LH2 crystal data though extensive computational simulations based on molecular dynamics (MD) and quantum chemical geometry optimization. A high computational expense of the quantum chemical geometric search is mitigated using our extended variant of the N-layered integrated molecular orbital and molecular mechanics (ONIOM)[58] method.

As written above, the advances in our spectrum simulation are thus two-fold: use of our dimer exciton model and refined crystal structure. These are fully exploited to explore the spectral tuning mechanism of LH2's absorption spectrum in such a way to develop a reliable foundation of theoretical analysis of LH2.

2. THEORETICAL METHODS

2.1. Exciton model

Here, we briefly explain the procedure for calculating absorption spectra using the exciton model. The details are described in Refs.[54, 57]. Let us here consider the total Hamiltonian of an assembly system consisting of N molecules, which is given by

$$\hat{H} = \sum_{i}^{N} \hat{H}_i + \sum_{i}^{N} \sum_{j>i}^{N} \hat{V}_{ij} \ , \qquad (1)$$

where $\hat{H}_i$ is the local Hamiltonian for the molecule i, and $\hat{V}_{ij}$ is the excitonic interaction between different molecules i and j. The exciton model is constructed from the basis represented by the direct product of the electronic states of N molecules

$$\left|\Phi_i^e\right\rangle = \left|\varphi_1^g \cdots \varphi_i^e \cdots \varphi_N^g\right\rangle \ , \qquad (2)$$

where φ_i^a represents the state a (a = ground state (g) or excited state (e)) of molecule i. This basis is also known as the diabatic state. For simplicity, let us consider two electronic states formed by molecules i and j (i.e., N = 2). These states are written as follows,

$$\begin{aligned} \left|\Phi_1\right\rangle &= \left|\varphi_i^e \cdot \varphi_j^g\right\rangle, \\ \left|\Phi_2\right\rangle &= \left|\varphi_i^g \cdot \varphi_j^e\right\rangle \end{aligned} \ , \qquad (3)$$

serving as the basis. Using these basis states (eq. (3)), the Hamiltonian (eq. (1)) can be written in form of the 2×2 matrix as,

$$\mathbf{H} = \begin{pmatrix} E_i & V_{ij} \\ V_{ji} & E_j \end{pmatrix} . \qquad (4)$$

Here, the diagonal element E_i corresponds to the electronic excitation energy of molecule *i*. The off-diagonal element V_{ij} is the excitonic coupling between molecules *i* and *j*.

As discussed earlier, there are various formalisms to calculate the excitonic coupling V_{ij}.[36-49] In this study, we use the TrESP method,[42, 51] in which V_{ij} is expressed by the classical Coulomb interaction between atomic transition charges

$$V_{ij} = \sum_{a \in i} \sum_{b \in j} \frac{q_a q_b}{r_{ab}} , \qquad (5)$$

where q_x ($x = a$ or b) denotes the transition charge for atom *x* in molecule *X* ($X = i$ or *j*) and r_{ab} is the interatomic distance between atoms *a* and *b*.

Numerical diagonalization of the Hamiltonian matrix **H** (eq. (4)) yields a spectrum of excited states of the total system, namely exciton states, as eigenstates. The *K*-th exciton state is expressed as a linear combination of basis states (eq. (3))

$$\left| \Psi_K \right\rangle = \sum_l C_{lK} \left| \Phi_l \right\rangle , \quad (6)$$

where the eigenvectors of **H** are used for the expansion coefficients C_{lK}. The associated eigenvalues serve as the exciton energies E_K. It is noted that the ground state energy is given as zero (i.e., $E_0 = 0$) and E_K matches the excitation energy of the *K*-th exciton state because in the present scheme, the diagonal elements of **H** are given by transition energies of the subsystems between their ground and excited states. The coefficients C_{lK} (eq. (6)) are used for converting the

transition dipole moments of the non-interacting subsystem $\boldsymbol{\mu}_l$ to the ones of the interacting (or total) system $\boldsymbol{\mu}'_K$ [51]

$$\boldsymbol{\mu}'_K = \sum_l C_{lK} \boldsymbol{\mu}_l \ . \qquad (7)$$

Given the transition moment and energy of the K-th exciton state, its oscillator strength is calculated to be

$$f_K = \frac{2}{3} E_K \left| \boldsymbol{\mu}'_K \right|^2 \ . \qquad (8)$$

Finally, the absorption spectrum is simulated using the following expression

$$\varepsilon(E) \propto \sum_K \frac{f_K E_K}{\sqrt{2\pi}\sigma} \exp\left[-\frac{\left(E - E_K\right)^2}{2\sigma^2} \right], \quad (9)$$

where the parameter σ denotes the standard deviation of the Gaussian distribution.

2.2. Dimer exciton model

The inclusion of the CT nature has to be considered for the sake of suitably charactering the exciton states of B850.[28] In this study, we introduce the extended exciton model, referred to as *dimer exciton model*, to allow us to incorporate the CT-type excitations into the representation of the exciton states.

The conventional exciton model built upon the monomeric local excitations is hereafter designated *monomer exciton model* in order to discriminate it from the dimer exciton model. As straightforwardly using eq. (2), the monomer exciton model is based on the representation of the

exciton state with a superposition of direct products of N local electronic states associated with N monomeric units. In modeling B850 assembly, as each BChl monomer acts as a local unit, 18 local excitations arising from B850's 18 BChl chromospheres constitute 18 basis states. With these basis, the Hamiltonian matrix is written as

$$\mathbf{H} = \begin{pmatrix} E_1 & V_{1,2} & \cdots & V_{1,18} \\ V_{2,1} & E_2 & \cdots & V_{2,18} \\ \vdots & \vdots & \ddots & \vdots \\ V_{18,1} & V_{18,2} & \cdots & E_{18} \end{pmatrix}, \qquad (10)$$

where the subscript of the matrix element represents the index of the BChl monomers.

At the heart of the dimer exciton model is to use dimeric electronic states as units in place of the monomeric states. Let us here suppose that a N-monomeric system is an assembly of $N/2$ dimers. For B850 (N = 18), the dimer exciton model is formulated using the first and second excited states of each of 9 BChl dimers. This again leads to 18×18 Hamiltonian matrix but with the reformulated elements, which are differentiated from eq. (10), as follows,

$$\mathbf{H} = \begin{pmatrix} E_1^{(1)} & 0 & \cdots & V_{1,9}^{(1,1)} & V_{1,9}^{(1,2)} \\ 0 & E_1^{(2)} & \cdots & V_{1,9}^{(2,1)} & V_{1,9}^{(2,2)} \\ \vdots & \vdots & \ddots & \vdots & \vdots \\ V_{9,1}^{(1,1)} & V_{9,1}^{(1,2)} & \cdots & E_9^{(1)} & 0 \\ V_{9,1}^{(2,1)} & V_{9,1}^{(2,2)} & \cdots & 0 & E_9^{(2)} \end{pmatrix}, \qquad (11)$$

where $E_X^{(i)}$ is the i-th excited state of dimer X (X = 1,2,…,9) and $V_{X,X'}^{(i,i')}$ is the excitonic coupling between the i-th excited state of dimer X and the i'-th excited state of dimer X'. It should be noted that the off-diagonal elements of the same dimer are set to zero, i.e., $V_{X,X}^{(i,i')} = 0$ ($i \neq i'$).

2.3. Relation to the *ab initio* exciton model

As mentioned in Introduction, Li et al. presented the *ab initio* exciton model that can additionally consider the CT effect, and used it to calculate the absorption spectrum of B850.[28] Here, however, it should be emphasized that in Ref. [57], four years earlier than Ref. [28], one of the authors (K.J.F.) proposed a method equivalent to the one by Li et al. The details of the method by Fujimoto et al., named TDFI-TI method, are described in Refs.[54, 57]. This *ab initio* exciton method by Fujimoto and Li *et al.* is somewhat different from the dimer exciton model introduced in Sec. 2.2 and applied to LH2 in the present study. In this section, we briefly explain differences between the dimer exciton model shown in Sec. 2.2 and the *ab initio* exciton model proposed in Refs.[54, 57] and applied to B850 in Ref. [28]

In the previous *ab initio* exciton model, the Hamiltonian matrix is constructed using two kinds of basis states: the one representing local excitation (LE) within a molecular fragment and the other representing CT between molecular fragments. In this model, an intermediate physical quantity called transfer integral, which involves electron transfer and hole transfer between molecular fragments, is incorporated into the exciton Hamiltonian as its off-diagonal matrix elements. This treatment makes it possible to take into account the mixing of LE and CT states.

The introduction of the CT basis into the exciton Hamiltonian, however, causes a negative feedback on the computational complexity of evaluating the matrix elements of the Hamiltonian matrix. A particularly cumbersome task is the evaluation of the transfer integrals. It is done using the configuration interaction (CI) coefficients of the LE states and the molecular orbital (MO) coefficients of each fragment, and may thus require extra tedious work for handling their data to calculate each single transfer integral. Because the number of the transfer integrals increases

quadratically with increasing molecular size, the *ab initio* exciton model for larger systems like LH2 becomes less applicable.

In contrast, in our dimer exciton model, the Hamiltonian matrix is constructed in a simple way based on using only LE basis states, which are actually dimeric states treated as *local* description. This LE basis thus allows us to inherently incorporate CT effects into the LE description. In other words, the electronic states of the dimer are solved by quantum chemical calculations, as in supermolecule calculations, and used as a basis for constructing the Hamiltonian matrix. Therefore, if CT excitations occur within the dimer used as the LE basis, the CT effects will already be incorporated into the LE basis. Importantly, this scheme does not require the modeling of explicit CT basis and concomitant evaluation of the transfer integrals. We thus view our *ab initio* dimer model as a simple but effective extension of the conventional exciton model towards the inclusion of the CT effect. Although the dimer exciton model cannot account for CT beyond the dimer, Coulomb couplings between dimers are included as in the monomer exciton model. As conventionally treated, the off-diagonal elements in this model are written only using the excitonic interactions V_{ij} (eq. (5)) between the LE states, which are again dimeric in our case. Note that the Coulomb couplings within the dimer are not included to avoid double counting, as shown in eq. (11). Thus, our approach is as simple as the conventional exciton model fully based on LE basis, as opposed to the previous *ab initio* model of Refs.[54, 57, 28]. In addition, it does not require complicated transfer integral calculations using any intermediate integrals and coefficient data of quantum chemistry calculations. Therefore, as a methodological strength, our dimer exciton model can be easily applied to larger systems including LH2.

2.4. Refinement of the crystal structure

The previously-reported spectral simulations on LH2 were solely performed with its atomic coordinates taken from the crystal structure without any refinement. The structural refinement, however, is considered to, in many cases, improve descriptions. In this study, our special attention is devoted to its effect on the excitation energy, which is examined with care. Our simulation-based refinement is outlined below.

The atomic coordinates of LH2 for the crystal structure were taken from PDB entry 1NKZ.[14] This structure was refined via two steps. First, a 100 ns MD simulation was performed on the LH2 protein and a 1-palmitoyl-2-oleoyl-phosphatidylethanolamine (POPE) membrane modeled in a periodic boundary box ($134 \times 133 \times 124$ Å^3) using a time step of 2 fs under NPT conditions at 300 K and 1 atm. The temperature was maintained using a Langevin thermostat,[59] and the particle mesh Ewald (PME) method[60] was applied to nonbonding interactions. The SHAKE method[61] was used for distance constraint of the bonds including hydrogens. The TIP3P,[62] ff14SB,[63] and lipid14[64] force fields were used for water molecules, the protein, and POPE, respectively.

Subsequently, the final MD structure was further refined by QM geometry optimization expedited by the ONIOM treatment,[58] in which the whole protein system was divided into QM and MM layers and they were described using density functional theory (DFT) with the B3LYP-GD3BJ functional[65-66] and the AMBER99 force field[67] for QM and MM methods, respectively. Handling all of 27 BChls of LH2 (**Figure 1b**) as a single QM system for the geometry optimization is extremely computationally demanding even using the ONIOM treatment. To mitigate this difficulty, the task was divided into several monomer-based geometry optimizations. The 27 BChls are separately optimized for every molecule by exploiting the ONIOM strategy where a single BChl is optimized at QM level of theory but the rest are treated at MM level of theory with their geometries unrelaxed. The separated optimizations went through all the BChls one time, and this

treatment seems to have a meaningful impact on geometric refinement. **Figure 1a** shows the optimized structure of LH2, which was directly used for the spectral calculations with the exciton model.

2.5. Computational details

The excitation energies and transition densities required for the exciton model calculations were obtained using time-dependent DFT with the ωB97X functional[68] (TD-ωB97X). The protein electrostatic effect was taken into account by means of the electronic embedding scheme employing the atomic MM charges offered by the Amber99 force field. The 6-311+G(2d,p) basis set was used for atomic basis functions throughout the QM calculations.

The Gaussian16 program package[69] was used to perform ONIOM geometry optimization on each of all the BChl monomers and to calculate excited states for each of all the BChl monomers and selected dimers. All MD simulations were performed with the AMBER 2019 program package[70].

The parameter σ that acts as the standard deviation of the spectrum broadening (eq. (9)) was set to 0.049 and 0.035 eV for B850 and B800, respectively.

3. RESULTS AND DISCUSSION

3.1. Excitation energies and excitonic couplings of BChls

This section begins by discussing the electronic structure of the isolated BChl monomer to ensure the basic understanding towards its aggregations. It is noted that there is no experimental

value for the excitation energy of the BChl monomer in the gas phase. **Figure 1(c)** shows the optimized structure of the BChl monomer in the gas phase. The excited state calculations were performed at TD-ωB97X level of theory, showing that the first excited state has a large oscillator strength (0.369 au) and is characterized as π–π* excitation from the highest occupied molecular orbital (HOMO) to the lowest unoccupied molecular orbital (LUMO). The excitation energy was calculated to be 1.628 eV (**Table 1**), which differs from the experimental values of B800 (1.550 eV) and B850 (1.459 eV) in LH2 complex by approximately 0.078 and 0.169 eV, respectively.

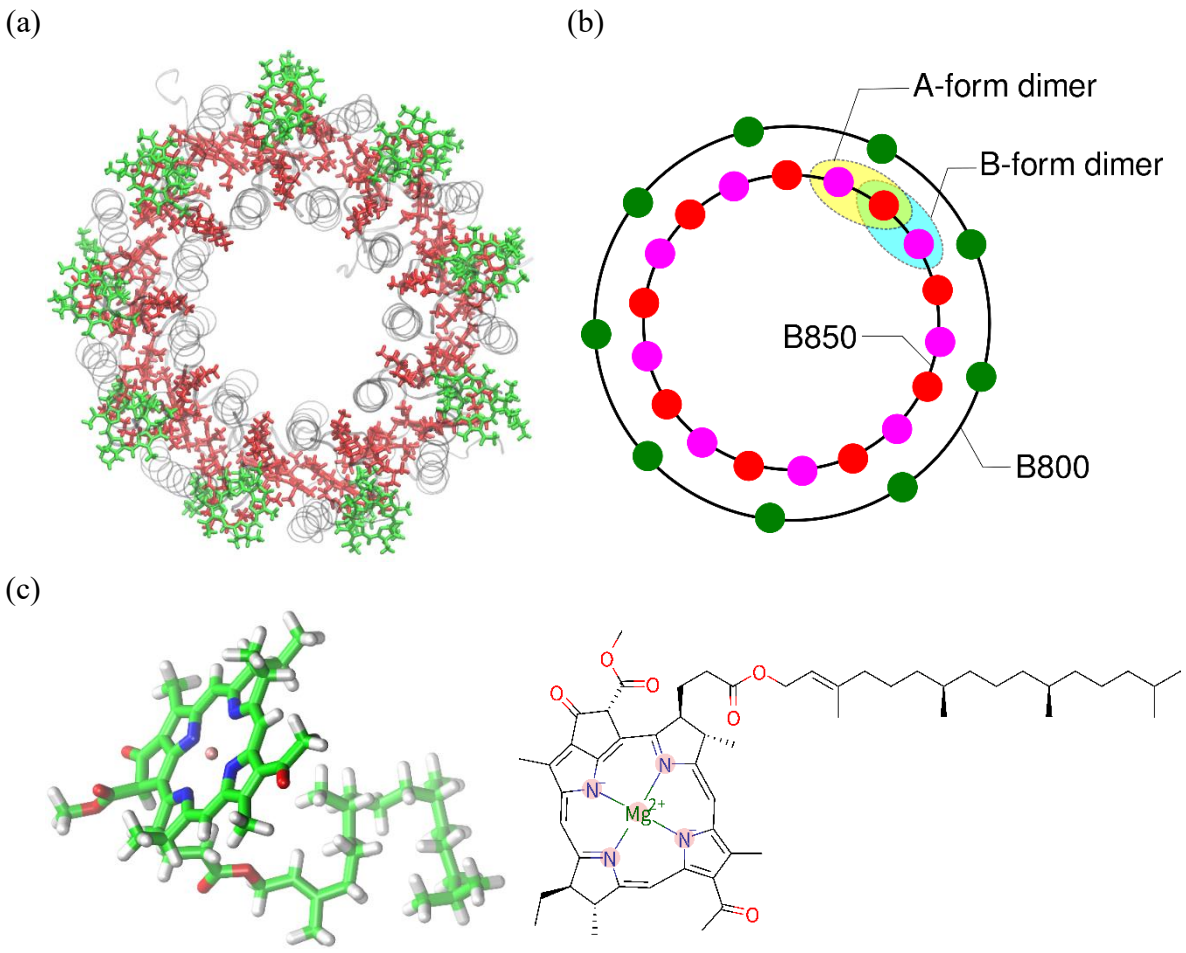

Figure 1. (a) Optimized structure of LH2. The structures of BChl in B850 and B800 are shown in red and green, respectively. (b) Schematic illustration of LH2. The B850 and B800 rings are assemblies of 18 and 9 BChls, respectively. For the dimer exciton model, A-form and B-form were considered, which correspond to intrachain and interchain dimer of B850, respectively. (c) Optimized structure of BChl in the gas phase along with its chemical structure.

Table 1. Excitation energies (E_{ex}) and excitonic coupling energies in absolute value ($|V|$) obtained with QM/MM and QM-only calculations for monomers and dimers of BChl in the optimized B850 and B800 structures. $|V|$ is calculated with the pairs of BChl monomers and dimers in the optimized structures. E_{ex} for the aggregate is shown with its average and standard deviation (SD).

BChl structure	E_{ex} [a]			$\|V\|$ (cm^{-1}) [b]
	Average		SD	
	(eV)	(nm)	(eV)	
B800 monomers	1.609 (1.628)	771 (762)	0.023 (0.025)	15.1~33.3
B850 monomers	1.588 (1.608)	781 (771)	0.030 (0.022)	8.1~403.6
B850 A-form dimers	1.506	823	0.023	1.0~319.8
B850 B-form dimers	1.575	787	0.028	-
B850 A-form dimers and B800	-	-	-	0.4~61.2
Isolated BChl (the fully relaxed BChl monomer) [c]	1.628	762	-	-

[a]Values in parenthesis are the results obtained with the structures in aggregations but by ignoring peripheral electrostatic effects. [b]Values for the neighboring pairs of the BChl monomers and dimers. [c]The structure optimized in the isolated and gas-phase condition; see also **Figure 1 (c)**.

When forming aggregations, BChls in the assembly are each structurally distorted relative to the gas-phase structure. Now, we turn to the effect of the structural distortion of BChl in LH2 on the excitation energy. To analyze it, the BChl monomer was isolated from the ONIOM optimized structure of LH2 with no geometric modification, and TD-ωB97X calculations were performed on it with each single molecule of the BChls treated in the gas phase. This approach allows us to extract the effect of the structural distortion of the molecules in the protein by comparing with the results shown previously for the fully relaxed monomer (i.e., "Isolated BChl" in **Table 1**). The calculated results are summarized in **Table 1**. The excitation energies of the 9 BChls of B800 range from 1.590 eV to 1.668 eV with an average of 1.628 eV and a standard deviation of 0.025 eV. The structure used here is extracted from the single optimized structure and is not an ensemble average of the various snapshots obtained from the MD simulations. This means that the protein disorder is ignored, and thus each excitation energy has a certain range. This average excitation energy is virtually the same as that of the fully relaxed monomer (1.628 eV). This indicates that the structural distortion of the BChls of B800 has little effect on its spectral shift. On the other hand, the excitation energies of the 18 BChls of B850 range from 1.554 eV to 1.664 eV with an average of 1.608 eV and a standard deviation of 0.022 eV. This average excitation energy is 0.020 eV smaller than that of the fully relaxed monomer, suggesting that the structural distortion of BChl contributes to the spectral redshift of B850 to some extent. However, the experimentally observed spectral shift of B850 cannot be explained by the distortion of the BChl structure alone.

A possible error correction that can readily be incorporated into the above analysis is the inclusion of the electrostatic effect of the protein environment. This effect was taken into account by the QM/MM scheme, in which we again performed the TD-ωB97X calculations on the distorted BChl monomers but with inclusion of the electrostatic potential of the surrounding system based

on the atomic MM point charges[71] (**Table 1**). The excitation energies of the 9 BChls of B800 range from 1.581 eV to 1.654 eV with an average of 1.609 eV and a standard deviation of 0.023 eV (See **Table S1**). On the other hand, the excitation energies of the 18 BChls of B850 range from 1.522 eV to 1.644 eV with an average of 1.588 eV and a standard deviation of 0.030 eV (See **Table S1**). These results show that the average excitation energies of B800 and B850 are smaller than those in the gas phase (1.628 eV for B800 and 1.608 eV for B850) by approximately 0.019 and 0.020 eV, respectively. This electrostatic correction plays a certain role; however, the corrected predictions remain away from the experimental absorption energies.

As seen in **Figure 1(a)**, the 18 BChl molecules of B850 are aggregated in close proximity to each other. It is hence speculated that the intermolecular interactions among the BChls in B850 should be substantial and thus largely contribute to the spectral shifts. To confirm this, we compared the excitation energies of the BChl dimers with those of the BChl monomers. The dimer calculations were carried out based on the division of the assembly into 9 pairs of BChls. There are effectively only two patterns of the division because the assembly is in a circular shape, as schematized in **Figure 1 (b)**. Hereinafter, these patterns are referred to as A-form and B-form, corresponding to intrachain and interchain dimer in Ref. [29], respectively. The TD-ωB97X calculations gave excitation energies of 1.458 to 1.528 eV for the BChl dimers of the A-form and 1.518 to 1.614 eV for those of the B-form. As compiled in **Table 1**, the average excitation energy for the A-form is 1.506 eV, which is 0.082 eV smaller than that of the BChl monomer in B850 (1.588 eV). This suggests that the dimerization effect with the A-form plays a critical role in the spectral redshift of B850. On the other hand, the average excitation energy of the B-form was 1.575 eV, revealing that they slightly differ from that of the BChl monomer in B850 (1.588 eV). This indicates that the dimerization in the B-form is ineffective in causing the spectral redshift of

B850. The intermolecular Mg–Mg distance of the dimers of the A-form (~9.3 Å) was smaller than that of the B-form (~9.6 Å) (See **Table S3**), corroborating that the A-form is favored to capture the dimerization effect. Therefore, we used A-form for the calculations shown later with the dimer exciton model. Our result is different from the previous study by Cupellini *et al.*[29] in which the contribution of CT was larger for the B-form (interchain dimer). This may reflect a difference between our LH2 structure and theirs, but we will not pursue this further in this paper. If the dimerization effect is large not only in the A-forms but also in the B-forms, the advantage of the dimer exciton model cannot be demonstrated. Fortunately, however, the dimerization effect in the B-form is negligible, so the dimer exciton model works effectively.

In what follows, we examined the excitonic couplings V_{ij} calculated using the TrESP method, focusing on the intra-assembly pairs of (1) B850 and (2) B800, as well as the inter-assembly interactions of (3) B850-B800. Although more accurate methods for calculating excitonic couplings than the TrESP method have been proposed, such as the TDFI method, we used the TrESP method because of the large number of combinations of BChl in LH2. As shown in **Table 1**, the excitonic couplings in absolute value are (1) 1.0 to 320 cm^{-1}, (2) 15.1 to 33.3 cm^{-1}, and (3) 0.4 to 61.2 cm^{-1}, for all the neighboring BCls pairs of the aforementioned three types of interactions. The intra-assembly excitonic coupling of B850 was estimated to be larger in absolute value than that of B800. This reflects that the intermolecular distances between BChls are shorter in B850 than in B800. The inter-assembly excitonic coupling was found to make non-negligible contributions to the exciton Hamiltonian (The details are summarized in **Table S2**).

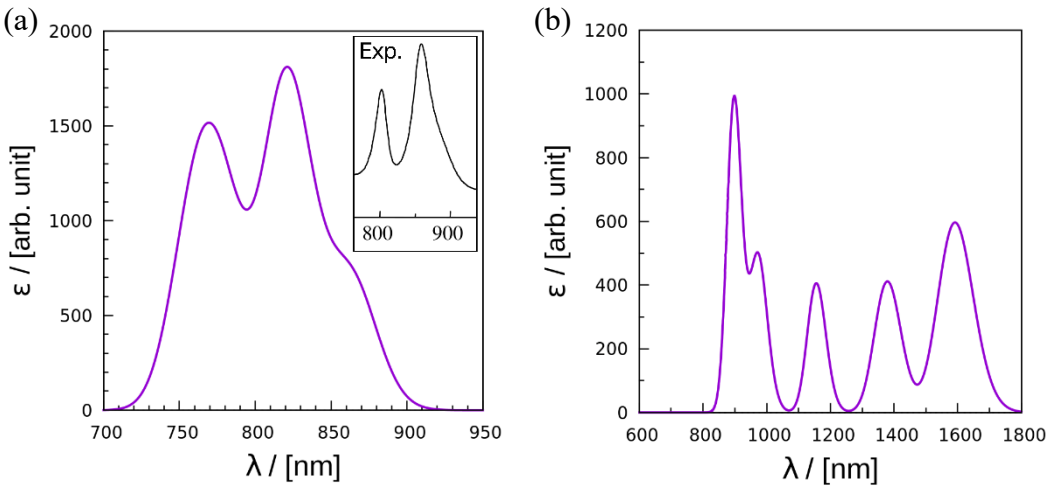

Figure 2. Theoretical absorption spectra of LH2 obtained with (a) the ONIOM optimized structure and (b) the crystal structure. The experimental absorption spectrum of LH2 is shown in the inset. It is taken from Fig. 3 of Ref. [15], reprinted with permission from Cambridge University Press.

3.2. Absorption spectrum calculated with the exciton model

Given the excitation energies of subsystems and excitonic couplings between them, presented in Sec. 3.1., we used them as parameters of the exciton model to simulate the absorption spectrum of LH2. As detailed in Sec. 2.2., the exciton Hamiltonian matrix can be constructed in a total of basis states arising from 18 BChls of B850 and 9 BChls of B800, thus resulting in the 27×27 matrix. The basis states associated with B850 and B800 were built based on the dimer and monomer exciton models, respectively. The absorption spectra were calculated using eqs. (7)-(9). Note that the effect of the vibronic interaction is not taken into account. **Figure 2** show that the absorption spectra predicted using the refined and crystal structures exhibit striking disagreement. The result using the 6-31G(d) basis set is shown in **Figure S1**. The two large peaks at 821 nm (1.510 eV) and 770 nm (1.610 eV) were confirmed in the spectrum simulation with the refined structure (**Figure**

2(a)). These peak positions are in fairly good agreement with the experimental values, 850 nm (1.459 eV) and 800 nm (1.550 eV), with an error of 0.051 and 0.060 eV, respectively. Contrarily, as shown in **Figure 2(b)**, the prediction based on crystal structure evidently suffer a catastrophic breakdown, showing five large peaks at 1591 nm (0.779 eV), 1379 nm (0.899 eV), 1156 nm (1.073 eV), 971 nm (1.277 eV), and 898 nm (1.381 eV). These results indicate that the refinement of the crystal structure enabled by ONIOM geometry optimization plays a critically indispensable role in the prediction of the spectrum. Although other groups have already used the ONIOM method for geometry optimization,[30-31] the dramatic improvement in the absorption spectra compared to the crystal structure has not been verified. The present examination is thus the first that has shown the importance of the structural refinement for the *ab initio* computational modeling of LH2.

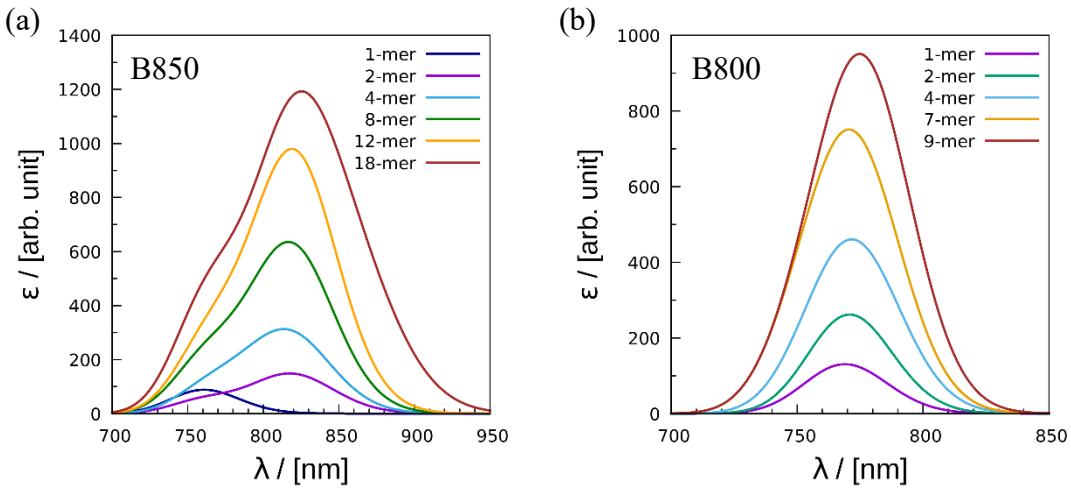

Figure 3. The theoretical absorption spectra of the BChl assemblies as a function of the number of BChls, which are of structures extracted from (a) B850 and (b) B800 assemblies, viewed as an 18-mer and 9-mer, respectively, in full form.

To examine the aggregation effect on the spectral shifts of B850 and B800 from a different approach, we simulated the absorption spectrum of the BChl assembly with varying number of BChls. The structures of the various-size assemblies were directly taken from the B850 and B800 as their parts, in which they are increasingly enlarged by appending neighboring B800 BChl monomers and B850 BChl A-form dimers. As shown in **Figure 3**, all the calculated spectra as a function of the number of BChls showed a large peak at varying wavelengths. For B850, this peak position was increasingly redshifted from 761 nm for the BChl monomer to 825 nm for the 18mer. For B800, an increasing redshift was again observed from 769 nm for the monomer to 775 nm for the 9mer. Similar results were obtained using the 6-31G(d) basis set (See **Figure S2**). These results clearly showed that the number of BChls in an assembly increasingly affects the shape of the absorption spectra of both B850 and B800.

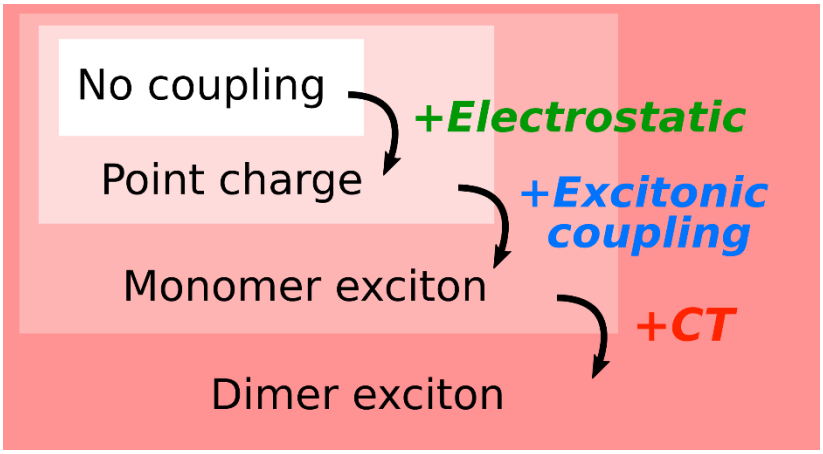

Figure 4. Schematic illustration of the four computational models employed for analyzing absorption spectra of B850 and B800.

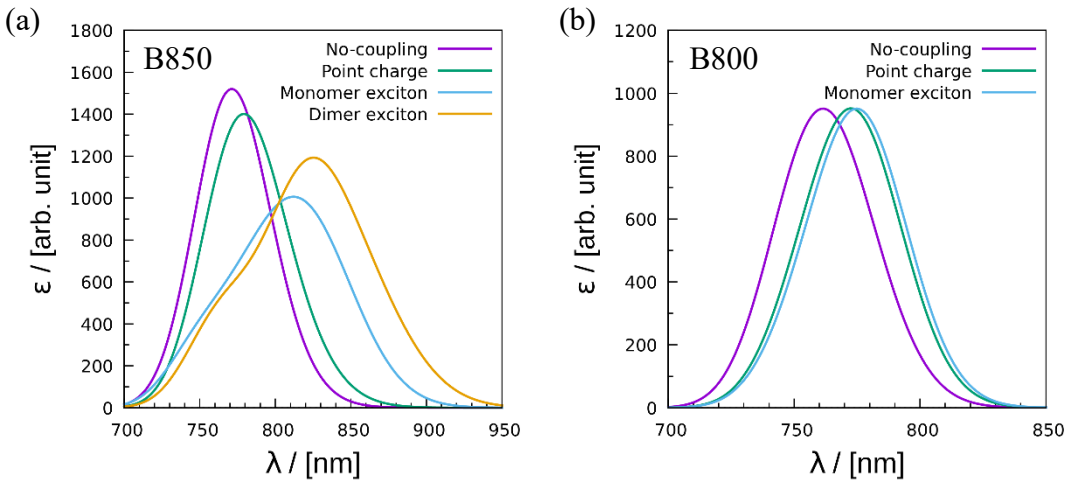

Figure 5. Theoretical absorption spectra of (a) B850 and (b) B800 calculated with the no-coupling model, point charge model, and monomer exciton model. For comparison, the absorption spectrum calculated with the dimer exciton model is included in (a).

Table 2. Simulated absorption energies (see also **Figure 5**) and experimental values of B850 and B800. The excitation energy of the BChl monomer in the gas phase with fully relaxed geometry was calculated to be 1.628 eV (762 nm), which can be considered as the starting point of the redshift common for B850 and B800.

	Model	eV	nm
B850	No coupling	1.608	771
	Point charge	1.592	779
	Monomer exciton	1.527	812
	Dimer exciton	1.503	825
	Exptl.	1.459	850
B800	No coupling	1.627	762
	Point charge	1.606	772
	Monomer exciton	1.600	775
	Exptl.	1.550	800

3.3. Mechanism of the spectral tuning

Our exciton model has offered highly reliable prediction of the experimental absorption wavelengths and the redshift effects on them in LH2's spectrum; therefore, the meaningful understanding of the spectral tuning mechanism can be derived based on our spectrum simulation. We here carried out the component analysis of the spectral redshifts of B850 and B800 in terms of gauging the contributions of the electrostatic effect, excitonic coupling effect, and CT effect. To

this end, we performed extra spectrum calculations using the no-coupling model, point charge model, and monomer exciton model on B850 and B800 separately with the ONIOM optimized structure. **Figure 4** briefly shows the difference between the four computational models. In this analysis, we ignored the inter-assembly excitonic coupling to calculate the absorption wavelengths for convenience.

The no-coupling model is viewed as formulated by Hamiltonian matrix containing only diagonal elements using the excitation energies of the BChl monomers in the gas phase. The point charge model is defined as the no-coupling model augmented with the electrostatic protein effect again for the diagonal elements. Comparing spectra simulated with the no-coupling model and point charge model allows us to measure the electrostatic effect on the redshift. As discussed earlier, the monomer exciton model certainly takes the environment effect in account; thus, the difference between the point charge model and monomer exciton model casts light on the effect of excitonic coupling. The CT effect can be estimated as the difference between the results obtained with the monomer and dimer exciton models.

The intermolecular Mg–Mg distances between BChls in B800 (~22 Å) are significantly larger than those in B850 (~9 Å). This suggests that the contribution of the CT effect to the B800 spectrum should be negligible. Indeed, the TD-ωB97X excitation energy calculated for the dimer of the nearest-neighbor BChls of B800 was different from that for the monomer by only approximately 0.003 eV. Therefore, the analysis of the CT contribution for B800 was excluded.

Figure 5 displays the simulated spectra for B850 and B800 as a function of the above models, and **Table 2** lists their absorption peaks along with the experimental values. It is noted that the values in **Table 2** are different from those in **Table 1**, because the effect of oscillator strength is

taken into account as well as the absorption energy. The peaks for B850 were obtained to be 1.608, 1.592, 1.527, and 1.503 eV by the no-coupling, point charge, monomer exciton, dimer exciton models, respectively, increasingly approaching the experimental value (1.459 eV), with increasing level of the models. The similar trend was observed for the peaks for B800, which were calculated to be 1.627, 1.606 and 1.600 eV by the no-coupling, point charge, and monomer exciton models, respectively, showing an increasing redshift towards the experimental value (1.550 eV). These results indicate that both the electrostatic and excitonic coupling effects contribute more or less to the redshift for B850 and B800, and the CT effect is also the case for B850.

Furthermore, the excitation energy of the BChl monomer in the gas phase with fully relaxed geometry (1.628 eV) is taken as the starting point of the spectral shift, which is common for B850 and B800; thus, the redshift of the absorption wavelengths of the no-coupling model relative to this starting point can also be attributed to the molecular structural distortion of the BChls.

By taking the difference in value between these absorption energies simulated with the different physical treatments, we obtained a quantitative decomposition of the redshift into the contributions of the structural distortion, electrostatic, excitonic coupling, and CT effects. The results of the component analysis are graphically represented in **Figure 6**. The striking finding is that the ratio distributions of the decomposed spectral shifts profoundly differ in character between B850 and B800. The major role in the spectral shift of B850 was played firstly by the excitonic coupling effect, giving a redshift of 0.065 eV, amounted to 52.0% of the shift energy, and secondly by the CT effect, yielding a redshift of 0.024 eV, accounting for another 19.2%. These intermolecular electronic interactions elucidated by quantum mechanical methods are thus totally weighted with over 70% for B850. On the other hand, for B800, these interactions are substantially lowered to 21.4%, which is in fact solely described by the excitonic coupling method with the CT effect

assumed to vanish. As seen in **Figure 6(c)**, the electrostatic effect arises as the main factor for B800, accounting for 75.0% of B800's total redshift (0.028 eV). Note that it can be treated classically.

Overall, our results have revealed that the spectral tunings simulated for B850 and B800 are driven by different physical origins, even though the two aggregates are built from the same molecular building blocks. The redshift mechanism for B850 is governed by intermolecular electronic interactions via quantum process including the CT to a significantly larger extent compared to B800, while that for B800 predominantly stems from classical electrostatic interactions with the protein environment.

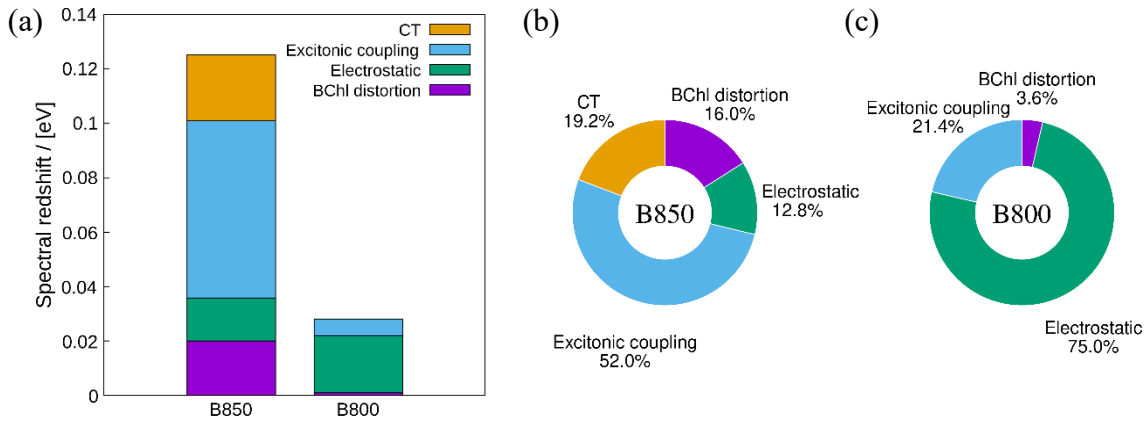

Figure 6. (a) Contributions to the spectral redshifts of B850 and B800 calculated by the decomposition of the shifted energy into the molecular structural distortion, electrostatic, excitonic coupling, and CT effects. Percentage of each contribution to the overall redshift of (b) B850 and (c) B800. The excitation energy of the BChl monomer with the fully-relaxed molecular geometry in the gas phase serves as the origin of the redshift.

4. CONCLUSIONS

In this paper, the extended exciton model in combination with the TrESP method has been proposed and applied to *ab initio* spectral simulation for the chromophore assemblies B850 and B800 embedded in LH2. Our simulation satisfactorily reproduced the experimental absorption spectra of B850 and B800, entailing the spectral redshift effects, with an error of 0.051 and 0.060 eV, respectively. What made this simulation possible is two-fold, lying in the applicability of our exciton model to the large system and the refinement of the crystal structure of LH2. To our best knowledge, our simulated spectrum is the first example to show that the QM-based geometry optimization using the ONIOM method is crucial for reproducing the absorption spectrum of LH2. On the basis of it, our approach further allows us to perform the component analysis on the spectral shift in order to systematically and quantitatively illuminate several physical factors that cause the spectral tuning in B850 and B800. Technologically, we used a newly-introduced extension of the exciton model based on the dimer fragmentation of the BChl assembly, which enabled an efficient prediction of photoabsorption energies and oscillator strengths of LH2.

In our simulation of the spectrum of LH2, we revealed a great importance of the refinement of the crystal structure. We refined the atomic geometries of the crystal structure through the extensive computational simulations using MD and quantum chemical geometry optimization. The earlier studies did not discuss the effect of the geometry optimization. We demonstrated that the use of the crystal structure of LH2 without any modification yielded the spectrum showing a completely different shape from the experimental spectrum. This error was markedly ameliorated by the use of the optimized structure. However, since the spectra in this study were calculated using only the single optimized structure, the effect of protein disorder on the spectra was ignored. Several studies perform MD simulations,[26-27, 29, 31] which effectively eliminate some of the crystal

structure issues and account for protein disorder, but have the disadvantage of introducing additional sources of error if the MD is based on a classical force field. Clarifying the relationship between these structures and the spectra is a future challenge.

Based on the calculated absorption maxima, we explored the spectral tuning mechanism in LH2 by decomposing the spectral shift relative to the monomer absorption energy into the contributions of BChl structural distortion, electrostatic, excitonic coupling, and CT effects. The analysis showed that for B850, the excitonic coupling between BChls is indispensable for the spectral redshift. A further analysis revealed that this CT effect is attributed to the presence of the closely-spaced BChl dimers. For B800, the electrostatic effect was found to be a main contribution to the redshift. One of the authors (K.J.F.) previously investigated the spectral tuning mechanism in retinal proteins and found that the degree of the electrostatic effect differs largely depending on the types of the protein environment, causing the difference in absorption peak of the retinal chromophore between them.[72-73] In contrast to this case, the present work has evinced that the difference in absorption peak between B850 and B800 in LH2 protein can be mainly explained by the degree of the excitonic coupling instead of the electrostatic modulation. This finding supports the hypothetical observation that every biomolecule adopts different physicochemical strategies for their spectral tuning and diversification of absorption wavelengths.

The *ab initio* dimer exciton model with the ONIOM-based structural refinement scheme appears to be a promising approach to the spectral calculation of LH2 or other kinds of photoactive biological aggregates. The results of our spectral simulation and analysis should serve as a basis for understanding the molecular origin of the spectral tuning in LH2. The high reliability and broad applicability of this approach will be useful for the analysis of the molecular mechanism of inter-chromophore interactions in photosynthetic antenna systems other than LH2.

ASSOCIATED CONTENT

Supporting Information.

The following file is available free of charge.

Details on the excitation energies, excitonic coupling energies, and Mg-Mg distances; Additional results of the excitation energies and absorption spectra; Geometric data for the optimized BChls (PDF)

AUTHOR INFORMATION

Notes

The authors declare no competing financial interests.

ACKNOWLEDGMENT

This study was supported by JSPS KAKENHI (Grant No. 20K05430 to KJF and 21H01881 to TY).

REFERENCES

1. Kazmaier, P. M.; Hoffmann, R., A Theoretical Study of Crystallochromy. Quantum Interference Effects in the Spectra of Perylene Pigments. *J. Am. Chem. Soc.* **1994,** *116*, 9684-9691.

2. Valdes-Aguilera, O.; Neckers, D. C., Aggregation Phenomena in Xanthene Dyes. *Acc. Chem. Res.* **1989,** *22*, 171-177.

3. de Diesbach, H.; von der Weid, E., Quelques sels complexes des o-dinitriles avec le cuivre et la pyridine. *Helv. Chim. Acta* **1927,** *10*, 886-888.

4. Lucia, E. A.; Verderame, F. D., Spectra of Polycrystalline Phthalocyanines in the Visible Region. *J. Chem. Phys.* **1968,** *48*, 2674-2681.

5. Scholes, G. D., Quantum-Coherent Electronic Energy Transfer: Did Nature Think of It First? *J. Phys. Chem. Lett.* **2010,** *1*, 2-8.

6. Scholes, G. D.; Fleming, G. R.; Olaya-Castro, A.; van Grondelle, R., Lessons from nature about solar light harvesting. *Nat. Chem.* **2011,** *3*, 763-774.

7. Adolphs, J.; Müh, F.; Madjet, M. E.; Schmidt am Busch, M.; Renger, T., Structure-Based Calculations of Optical Spectra of Photosystem I Suggest an Asymmetric Light-Harvesting. *J. Am. Chem. Soc.* **2010,** *132*, 3331-3343.

8. Cassim, J. Y., Unique biphasic band shape of the visible circular dichroism of bacteriorhodopsin in purple membrane. *Biophys. J.* **1992,** *63*, 1432-1442.

9. Georgakopoulou, S.; van Grondelle, R.; van der Zwan, G., Circular Dichroism of Carotenoids in Bacterial Light-Harvesting Complexes: Experiments and Modeling. *Biophys. J.* **2004,** *87*, 3010-3022.

10. Cheng, Y.-C.; Fleming, G. R., Dynamics of Light Harvesting in Photosynthesis. *Annu. Rev. Phys. Chem.* **2009,** *60*, 241-262.

11. Saito, S.; Higashi, M.; Fleming, G. R., Site-Dependent Fluctuations Optimize Electronic Energy Transfer in the Fenna–Matthews–Olson Protein. *J. Phys. Chem. B* **2019,** *123*, 9762-9772.

12. McDermott, G.; Prince, S. M.; Freer, A. A.; Hawthornthwaite-Lawless, A. M.; Papiz, M. Z.; Cogdell, R. J.; Isaacs, N. W., Crystal structure of an integral membrane light-harvesting complex from photosynthetic bacteria. *Nature* **1995,** *374*, 517-521.

13. Koepke, J.; Hu, X.; Muenke, C.; Schulten, K.; Michel, H., The crystal structure of the light-harvesting complex II (B800–850) from Rhodospirillum molischianum. *Structure* **1996,** *4*, 581-597.

14. Papiz, M. Z.; Prince, S. M.; Howard, T.; Cogdell, R. J.; Isaacs, N. W., The Structure and Thermal Motion of the B800–850 LH2 Complex from *Rps. acidophila* at 2.0 Å Resolution and 100 K: New Structural Features and Functionally Relevant Motions. *J. Mol. Biol.* **2003,** *326*, 1523-1538.

15. Cogdell, R. J.; Gall, A.; Köhler, J., The architecture and function of the light-harvesting apparatus of purple bacteria: from single molecules to *in vivo* membranes. *Q. Rev. Biophys.* **2006,** *39*, 227-324.

16. Polívka, T.; Zigmantas, D.; Herek, J. L.; He, Z.; Pascher, T.; Pullerits, T.; Cogdell, R. J.; Frank, H. A.; Sundström, V., The Carotenoid S_1 State in LH2 Complexes from Purple Bacteria *Rhodobacter sphaeroides* and *Rhodopseudomonas acidophila*: S_1 Energies, Dynamics, and Carotenoid Radical Formation. *J. Phys. Chem. B* **2002,** *106*, 11016-11025.

17. Polli, D.; Cerullo, G.; Lanzani, G.; De Silvestri, S.; Hashimoto, H.; Cogdell, R. J., Carotenoid-Bacteriochlorophyll Energy Transfer in LH2 Complexes Studied with 10-fs Time Resolution. *Biophys. J.* **2006,** *90*, 2486-2497.

18. Cong, H.; Niedzwiedzki, D. M.; Gibson, G. N.; LaFountain, A. M.; Kelsh, R. M.; Gardiner, A. T.; Cogdell, R. J.; Frank, H. A., Ultrafast Time-Resolved Carotenoid to-Bacteriochlorophyll Energy Transfer in LH2 Complexes from Photosynthetic Bacteria. *J. Phys. Chem. B* **2008,** *112*, 10689-10703.

19. Yoneda, Y.; Noji, T.; Katayama, T.; Mizutani, N.; Komori, D.; Nango, M.; Miyasaka, H.; Itoh, S.; Nagasawa, Y.; Dewa, T., Extension of Light-Harvesting Ability of Photosynthetic Light-Harvesting Complex 2 (LH2) through Ultrafast Energy Transfer from Covalently Attached Artificial Chromophores. *J. Am. Chem. Soc.* **2015,** *137*, 13121-13129.

20. Hu, X.; Ritz, T.; Damjanović, A.; Schulten, K., Pigment Organization and Transfer of Electronic Excitation in the Photosynthetic Unit of Purple Bacteria. *J. Phys. Chem. B* **1997,** *101*, 3854-3871.

21. Alden, R. G.; Johnson, E.; Nagarajan, V.; Parson, W. W.; Law, C. J.; Cogdell, R. G., Calculations of Spectroscopic Properties of the LH2 Bacteriochlorophyll-Protein Antenna Complex from *Rhodopseudomonas acidophila*. *J. Phys. Chem. B* **1997,** *101*, 4667-4680.

22. Damjanović, A.; Ritz, T.; Schulten, K., Energy transfer between carotenoids and bacteriochlorophylls in light-harvesting complex II of purple bacteria. *Phys. Rev. E* **1999,** *59*, 3293-3311.

23. Scholes, G. D.; Gould, I. R.; Cogdell, R. J.; Fleming, G. R., *Ab Initio* Molecular Orbital Calculations of Electronic Couplings in the LH2 BacterialLight-Harvesting Complex of *Rps. Acidophila*. *J. Phys. Chem. B* **1999,** *103*, 2543-2553.

24. Linnanto, J.; Freiberg, A.; Korppi-Tommola, J., Quantum Chemical Simulations of Excited-State Absorption Spectraof Photosynthetic Bacterial Reaction Center and Antenna Complexes. *J. Phys. Chem. B* **2011,** *115*, 5536-5544.

25. van der Vegte, C. P.; Prajapati, J. D.; Kleinekathöfer, U.; Knoester, J.; Jansen, T. L. C., Atomistic Modeling of Two-Dimensional Electronic Spectra and Excited-State Dynamics for a Light Harvesting 2 Complex. *J. Phys. Chem. B* **2015,** *119*, 1302-1313.

26. Cupellini, L.; Jurinovich, S.; Campetella, M.; Caprasecca, S.; Guido, C. A.; Kelly, S. M.; Gardiner, A. T.; Cogdell, R.; Mennucci, B., An *Ab Initio* Description of the Excitonic Properties of LH2 and Their Temperature Dependence. *J. Phys. Chem. B* **2016,** *120*, 11348-11359.

27. Segatta, F.; Cupellini, L.; Jurinovich, S.; Mukamel, S.; Dapor, M.; Taioli, S.; Garavelli, M.; Mennucci, B., A Quantum Chemical Interpretation of Two-Dimensional Electronic Spectroscopy of Light-Harvesting Complexes. *J. Am. Chem. Soc.* **2017,** *139*, 7558-7567.

28. Li, X.; Parrish, R. M.; Liu, F.; Schumacher, S. I. L. K.; Martínez, T. J., An Ab Initio Exciton Model Including Charge-Transfer Excited States. *J. Chem. Theory Comput.* **2017,** *13*, 3493-3504.

29. Cupellini, L.; Caprasecca, S.; Guido, C. A.; Müh, F.; Renger, T.; Mennucci, B., Coupling to Charge Transfer States is the Key to Modulate the Optical Bands for Efficient Light Harvesting in Purple Bacteria. *J. Phys. Chem. Lett.* **2018,** *9*, 6892-6899.

30. Nottoli, M.; Jurinovich, S.; Cupellini, L.; Gardiner, A. T.; Cogdell, R.; Mennucci, B., The role of charge-transfer states in the spectral tuning of antenna complexes of purple bacteria. *Photosynth. Res.* **2018,** *137*, 215-226.

31. Bold, B. M.; Sokolov, M.; Maity, S.; Wanko, M.; Dohmen, P. M.; Kranz, J. J.; Kleinekathöfer, U.; Höfener, S.; Elstner, M., Benchmark and performance of long-rangecorrected time-dependent density functional tight binding (LC-TD-DFTB) on rhodopsins and light-harvesting complexes. *Phys. Chem. Chem. Phys.* **2020,** *20*, 10500-10518.

32. Frenkel, J., On the Transformation of Light into Heat in Solids. II. *Phys. Rev.* **1931,** *37*, 1276-1294.

33. May, V.; Kühn, O., *Charge and Energy Transfer Dynamics in Molecular Systems*. 3rd ed.; Wiley-VCH: Weinheim, 2011.

34. Förster, T., Zwischenmolekulare Energiewanderung und Fluoreszenz. *Ann. Phys.* **1948,** *437*, 55-75.

35. Speiser, S., Photophysics and Mechanisms of Intramolecular Electronic Energy Transfer in Bichromophoric Molecular Systems: Solution and Supersonic Jet Studies. *Chem. Rev.* **1996,** *96*, 1953-1976.

36. Chang, J. C., Monopole effects on electronic excitation interactions between large molecules. I. Application to energy transfer in chlorophylls. *J. Chem. Phys.* **1977,** *67*, 3901-3909.

37. Krueger, B. P.; Scholes, G. D.; Fleming, G. R., Calculation of Couplings and Energy-Transfer Pathways between the Pigments of LH2 by the ab Initio Transition Density Cube Method. *J. Phys. Chem. B* **1998,** *102*, 5378-5386.

38. Tretiak, S.; Middleton, C.; Chernyak, V.; Mukamel, S., Exciton Hamiltonian for the Bacteriochlorophyll System in the LH2 Antenna Complex of Purple Bacteria. *J. Phys. Chem. B* **2000,** *104*, 4519-4528.

39. Hsu, C.-P.; Fleming, G. R.; Head-Gordon, M.; Head-Gordon, T., Excitation energy transfer in condensed media. *J. Chem. Phys.* **2001,** *114*, 3065-3072.

40. Iozzi, M. F.; Mennucci, B.; Tomasi, J.; Cammi, R., Excitation energy transfer (EET) between molecules in condensed matter: A novel application of the polarizable continuum model (PCM). *J. Chem. Phys.* **2004,** *120*, 7029-7040.

41. Wong, K. F.; Bagchi, B.; Rossky, P. J., Distance and Orientation Dependence of Excitation Transfer Rates in Conjugated Systems: Beyond the Förster Theory. *J. Phys. Chem. A* **2004,** *108*, 5752-5763.

42. Madjet, M. E.; Abdurahman, A.; Renger, T., Intermolecular Coulomb Couplings from Ab Initio Electrostatic Potentials: Application to Optical Transitions of Strongly Coupled Pigments in Photosynthetic Antennae and Reaction Centers. *J. Phys. Chem. B* **2006,** *110*, 17268-17281.

43. Neugebauer, J., Couplings between electronic transitions in a subsystem formulation of time-dependent density functional theory. *J. Chem. Phys.* **2007,** *126*, 134116.

44. Fückel, B.; Köhn, A.; Harding, M. E.; Diezemann, G.; Hinze, G.; Basché, T.; Gauss, J., Theoretical investigation of electronic excitation energy transfer in bichromophoric assemblies. *J. Chem. Phys.* **2008,** *128*, 074505.

45. Fink, R. F.; Pfister, J.; Zhao, H. M.; Engels, B., Assessment of quantum chemical methods and basis sets for excitation energy transfer. *Chem. Phys.* **2008,** *346*, 275-285.

46. Vura-Weis, J.; Newton, M. D.; Wasielewski, M. R.; Subotnik, J. E., Characterizing the Locality of Diabatic States for Electronic Excitation Transfer By Decomposing the Diabatic Coupling. *J. Phys. Chem. C* **2010,** *114*, 20449-20460.

47. Kawatsu, T.; Matsuda, K.; Hasegawa, J., Bridge-Mediated Excitation Energy Transfer Pathways through Protein Media: a Slater Determinant-Based Electronic Coupling Calculation Combined with Localized Molecular Orbitals. *J. Phys. Chem. A* **2011,** *115*, 10814-10822.

48. Voityuk, A. A., Estimation of Electronic Coupling for Photoinduced Charge Separation and Charge Recombination Using the Fragment Charge Difference Method. *J. Phys. Chem. C* **2013,** *117*, 2670-2675.

49. Błasiak, B.; Maj, M.; Cho, M.; Góra, R. W., Distributed Multipolar Expansion Approach to Calculation of Excitation Energy Transfer Couplings. *J. Chem. Thory Comput.* **2015,** *11*, 3259-3266.

50. Fujimoto, K. J.; Hayashi, S., Electronic Coulombic Coupling of Excitation-Energy Transfer in Xanthorhodopsin. *J. Am. Chem. Soc.* **2009,** *131*, 14152-14153.

51. Fujimoto, K. J., Transition-density-fragment interaction approach for exciton-coupled circular dichroism spectra. *J. Chem. Phys.* **2010,** *133*, 124101.

52. Fujimoto, K. J., Transition-density-fragment interaction combined with transfer integral approach for excitation-energy transfer via charge-transfer states. *J. Chem. Phys.* **2012,** *137*, 034101.

53. Fujimoto, K. J., Electronic coupling calculations with transition charges, dipoles, and quadrupoles derived from electrostatic potential fitting. *J. Chem. Phys.* **2014,** *141*, 214105.

54. Fujimoto, K. J., Theoretical Calculations of Excitation Energy Transfer. In *Chemical Science of π-Electron Systems*, Akasaka, T.; Osuka, A.; Fukuzumi, S.; Kandori, H.; Aso, Y., Eds. Springer: Tokyo, Japan, 2015; pp 761-777.

55. Fujimoto, K. J.; Balashov, S. P., Vibronic coupling effect on circular dichroism spectrum: Carotenoid–retinal interaction in xanthorhodopsin. *J. Chem. Phys.* **2017,** *146*, 095101.

56. Fujimoto, K. J.; Inoue, K., Excitonic coupling effect on the circular dichroism spectrum of sodium-pumping rhodopsin KR2. *J. Chem. Phys.* **2020,** *153*, 045101.

57. Fujimoto, K. J.; Kitamura, C., A theoretical study of crystallochromy: Spectral tuning of solid-state tetracenes. *J. Chem. Phys.* **2013,** *139*, 084511.

58. Svensson, M.; Humbel, S.; Froese, R. D. J.; Matsubara, T.; Sieber, S.; Morokuma, K., ONIOM: A Multilayered Integrated MO+MM Method for Geometry Optimizations and Single Point Energy Predictions. A Test for Diels-Alder Reactions and $Pt(P(t\text{-}Bu)_3)_2+H_2$ Oxidative Addition. *J. Phys. Chem.* **1996,** *100*, 19357-19363.

59. Loncharich, R. J.; Brooks, B. R.; Pastor, R. W., Langevin dynamics of peptides: The frictional dependence of isomerization rates of N-actylananyl-N'-methylamide. *Biopolymers* **1992,** *32*, 523-535.

60. Darden, T.; York, D.; Pedersen, L., Particle mesh Ewald--an Nlog(N) method for Ewald sums in large systems. *J. Chem. Phys.* **1993,** *98*, 10089-10092.

61. Ryckaert, J.-P.; Ciccotti, G.; Berendsen, H. J. C., Numerical integration of the cartesian equations of motion of a system with constraints: Molecular dynamics of n-alkanes. *J. Comput. Phys.* **1977,** *23*, 327-341.

62. Jorgensen, W. L.; Chandreskhar, J.; Madura, J. D.; Impey, R. W.; Klein, M. L., Comparison of simple potential functions for simulating liquid water. *J. Chem. Phys.* **1983,** *79*, 926-935.

63. Maier, J. A.; Martinez, C.; Kasavajhala, K.; Wickstrom, L.; Hauser, K. E.; Simmerling, C., ff14SB: Improving the Accuracy of Protein Side Chain and Backbone Parameters from ff99SB. *J. Chem. Theory Comput.* **2015,** *11*, 3696-3713.

64. Dickson, C. J.; Madej, B. D.; Skjevik, Å. A.; Betz, R. M.; Teigen, K.; Gould, I. R.; Walker, R. C., Lipid14: The Amber Lipid Force Field. *J. Chem. Theory Comput.* **2014,** *10*, 865-879.

65. Lee, C.; Yang, W.-T.; Parr, R. G., Development of the Colle-Salvetti correlation-energy formula into a functional of the electron density. *Phys. Rev. B* **1988,** *37*, 785-789.

66. Grimme, S.; Ehrlich, S.; Goerigk, L., Effect of the Damping Function in Dispersion Corrected Density Functional Theory. *J. Comput. Chem.* **2011,** *32*, 1456-1465.

67. Wang, J.; Cieplak, P.; Kollman, P. A., How Well Does a Restrained Electrostatic Potential (RESP) Model Perform in Calculating Conformational Energies of Organic and Biological Molecules? *J. Comput. Chem.* **2000,** *21*, 1049-1074.

68. Chaia, J.-D.; Head-Gordon, M., Systematic optimization of long-range corrected hybrid density functionals. *J. Chem. Phys.* **2008,** *128*, 084106.

69. Frisch, M. J.; Trucks, G. W.; Schlegel, H. B.; Scuseria, G. E.; Robb, M. A.; Cheeseman, J. R.; Scalmani, G.; Barone, V.; Petersson, G. A.; Nakatsuji, H., et al. *Gaussian16*, Rev. C.01; Gaussian, Inc.: Wallingford, CT, 2019.

70. Case, D. A.; Ben-Shalom, I. Y.; Brozell, S. R.; Cerutti, D. S.; Cheatham, T. E., III; Cruzeiro, V. W. D.; Darden, T. A.; Duke, R. E.; Ghoreishi, D.; Giambasu, G., et al. *AMBER 2019*, University of California: San Francisco, CA, 2019.

71. Warshel, A.; Levitt, M., Theoretical Studies of Enzymic Reactions: Dielectric, Electrostatic and Steric Stabilization of the Carbonium Ion in the Reaction of Lysozyme. *J. Mol. Biol.* **1976,** *103*, 227-249.

72. Fujimoto, K.; Hayashi, S.; Hasegawa, J.; Nakatsuji, H., Theoretical Studies on the Color-Tuning Mechanism in Retinal Proteins. *J. Chem. Theory Comput.* **2007,** *3*, 605-618.

73. Fujimoto, K.; Hasegawa, J.; Nakatsuji, H., Color Tuning Mechanism of Human Red, Green, and Blue Cone Pigments: SAC-CI Theoretical Study. *Bull. Chem. Soc. Jpn.* **2009,** *82*, 1140-1148.

TOC GRAPHICS